NeuroImage 245 (2021) 118752

Contents lists available at ScienceDirect

NeuroImage

journal homepage: www.elsevier.com/locate/neuroimage

MR imaging for the quantitative assessment of brain iron in aceruloplasminemia: A postmortem validation study

Lena H.P. Vroegindeweij[a], Piotr A. Wielopolski[b], Agnita J.W. Boon[c], J.H. Paul Wilson[a], Rob M. Verdijk[d], Sipeng Zheng[e], Sylvestre Bonnet[e], Lucia Bossoni[f], Louise van der Weerd[f,g], Juan A. Hernandez-Tamames[b], Janneke G. Langendonk[a,*]

[a] *Department of Internal Medicine, Center for Lysosomal and Metabolic Diseases, Porphyria Center Rotterdam, Erasmus University Medical Center, Erasmus MC, Rotterdam, the Netherlands*
[b] *Department of Radiology and Nuclear Medicine, Erasmus University Medical Center, Erasmus MC, Rotterdam, the Netherlands*
[c] *Department of Neurology, Erasmus University Medical Center, Erasmus MC, Rotterdam, the Netherlands*
[d] *Department of Pathology, Erasmus University Medical Center, Erasmus MC, Rotterdam, the Netherlands*
[e] *Leiden Institute of Chemistry, Leiden University, Leiden, the Netherlands*
[f] *C.J. Gorter Center for High field MRI, Department of Radiology, Leiden University Medical Center, Leiden, the Netherlands*
[g] *Department of Human Genetics, Leiden University Medical Center, Leiden, the Netherlands*

ARTICLE INFO

Keywords:
Aceruloplasminemia
Neurodegeneration with brain iron accumulation (NBIA)
Postmortem MRI
Iron
Transverse relaxation rate (R_2^*)
Susceptibility
Ferritin

ABSTRACT

Aims: Non-invasive measures of brain iron content would be of great benefit in neurodegeneration with brain iron accumulation (NBIA) to serve as a biomarker for disease progression and evaluation of iron chelation therapy. Although magnetic resonance imaging (MRI) provides several quantitative measures of brain iron content, none of these have been validated for patients with a severely increased cerebral iron burden. We aimed to validate R_2^* as a quantitative measure of brain iron content in aceruloplasminemia, the most severely iron-loaded NBIA phenotype.

Methods: Tissue samples from 50 gray- and white matter regions of a postmortem aceruloplasminemia brain and control subject were scanned at 1.5 T to obtain R_2^*, and biochemically analyzed with inductively coupled plasma mass spectrometry. For gray matter samples of the aceruloplasminemia brain, *sample* R_2^* values were compared with postmortem *in situ* MRI data that had been obtained from the same subject at 3 T – *in situ* R_2^*. Relationships between R_2^* and tissue iron concentration were determined by linear regression analyses.

Results: Median iron concentrations throughout the whole aceruloplasminemia brain were 10 to 15 times higher than in the control subject, and R_2^* was linearly associated with iron concentration. For gray matter samples of the aceruloplasminemia subject with an iron concentration up to 1000 mg/kg, 91% of variation in R_2^* could be explained by iron, and *in situ* R_2^* at 3 T and *sample* R_2^* at 1.5 T were highly correlated. For white matter regions of the aceruloplasminemia brain, 85% of variation in R_2^* could be explained by iron.

Conclusions: R_2^* is highly sensitive to variations in iron concentration in the severely iron-loaded brain, and might be used as a non-invasive measure of brain iron content in aceruloplasminemia and potentially other NBIA disorders.

1. Introduction

Aceruloplasminemia (OMIM #604290) is a rare form of neurodegeneration with brain iron accumulation (NBIA), caused by homozygous or compound heterozygous mutations in the ceruloplasmin (*CP*) gene. The absence of functioning ceruloplasmin impairs cellular iron efflux and leads to excess cytotoxic iron accumulation in the central nervous system and in visceral organs (Miyajima et al., 2003). Postmortem studies in aceruloplasminemia have reported a five- to tenfold increase in brain iron concentrations compared to healthy individuals (Miyajima et al., 2003; Morita et al., 1995), predominantly affecting deep gray matter structures and cortex. Reliable, non-invasive measures of brain iron content would be of great benefit in NBIA to serve as a biomarker for disease progression and evaluation of iron chelation therapy.

Magnetic resonance imaging (MRI) provides several quantitative measures of brain iron content. The transverse relaxation rate R_2^* ($1/T_2^*$) has shown a strong linear association with biochemically de-

Abbreviations: NBIA, Neurodegeneration with Brain Iron Accumulation; *CP*, ceruloplasmin; ICP-MS, inductively coupled plasma mass spectrometry; UTE, ultrashort echo time; QSM, Quantitative Susceptibility Mapping; ROI, Region of interest.

* Corresponding author.

https://doi.org/10.1016/j.neuroimage.2021.118752.
Received 18 July 2021; Received in revised form 15 October 2021; Accepted 20 November 2021
Available online 22 November 2021.

termined iron concentrations in healthy gray matter brain structures (Langkammer et al., 2010; Stuber et al., 2014; Hametner et al., 2018), and has recently been validated as a measure for cortical iron content in Alzheimer's disease (Bulk et al., 2020). However, no validated measure exists for patients with a severely increased cerebral iron burden (Dusek et al., 2014; Löbel et al., 2014).

T_2^* reflects the decay of transverse magnetization that results from magnetic interactions between adjacent hydrogen protons (spin–spin relaxation) and inhomogeneities in the local magnetic field. Paramagnetic iron particles cause local magnetic field gradients and subsequent signal loss on T_2^*-weighted images (Chavhan et al., 2009). Tissue iron concentration has been shown to be an important determinant of T_2^* and its inverse R_2^* (Langkammer et al., 2010; Stuber et al., 2014; Bulk et al., 2020). However, several other factors contribute to T_2^* contrast, such as size, chemical form, spatial distribution, clustering of iron particles (Li et al., 2009; Gossuin et al., 2007; Tanimoto et al., 2001), and myelin (Stuber et al., 2014; Hametner et al., 2018; Li et al., 2009). The relative contribution of these sources to T_2^* contrast in heavily iron-loaded conditions is unknown. As such, the relationship between R_2^* and brain iron concentrations in healthy individuals and patients with Alzheimer's disease should not be directly extrapolated to diseases with severe brain iron overload, such as aceruloplasminemia and other NBIA disorders. Nevertheless, R_2^* is increasingly used as a measure of brain iron content in NBIA disorders (Löbel et al., 2014; Klopstock et al., 2019; Zhou et al., 2020; Pan et al., 2011; Zorzi et al., 2011; Cossu et al., 2014; Abbruzzese et al., 2011), with reductions in R_2^* being considered as an absolute proof of reductions in brain iron content of affected gray matter structures due to a successful iron chelation strategy (Löbel et al., 2014; Klopstock et al., 2019; Pan et al., 2011; Zorzi et al., 2011; Cossu et al., 2014; Abbruzzese et al., 2011).

The primary aim of our study was to establish the relationship between R_2^* and brain iron content in aceruloplasminemia, and to reflect on the suitability of R_2^*as a non-invasive measure of brain iron content in NBIA disorders. For this purpose, tissue samples from 50 gray- and white matter regions of a postmortem aceruloplasminemia brain and control subject were scanned at 1.5 T and biochemically analyzed with inductively coupled plasma mass spectrometry (ICP-MS). In addition, R_2^* values obtained from gray matter samples of the aceruloplasminemia brain were compared with postmortem *in situ* MRI data that had been obtained from the same subject, to disentangle influences of formalin fixation.

2. Materials and methods

2.1. Subjects

Formalin-fixed brain slabs from one deceased aceruloplasminemia patient (52 years, male) (Vroegindeweij et al., 2015; Vroegindeweij et al., 2017; Kerkhof and Honkoop, 2014; Vroegindeweij et al., 2020; Vroegindeweij et al., 2021) and one control subject (43 years, male) were obtained from the Department of Pathology, Erasmus University Medical Center, Erasmus MC, Rotterdam, The Netherlands. The subjects were matched based on age, gender and duration of fixation in 4% phosphate buffered formaldehyde, which was 5 years for the aceruloplasminemia patient and 4.5 years for the control case. The formalin was not renewed during these years. Autopsy was performed within 48 h of death. The brains were cut into 10 mm coronal slabs for pathological investigation, which revealed mild cerebral ischemic abnormalities in both cases. The control subject had no history of neurological disease, and was known with a soft tissue sarcoma. The study of the patient with aceruloplasminemia was approved by the Medical Ethics Review Board of the Erasmus MC, and his legal representative provided written informed consent. The control subject provided written informed consent for the secondary use of the tissue for research purposes, and all tissue was handled in a coded fashion according to the Dutch National Ethical Guidelines (Code for Proper Secondary Use of Human Tissue, Dutch Federation of Medical Scientific Societies).

2.2. Sample dissection

To avoid contamination with iron, all samples were dissected with a ceramic knife and any tissue that could have been in contact with iron-containing instruments during the autopsy procedure was removed. From both subjects, 50 tissue blocks of approximately 5 mm^3 were dissected from gray and white matter regions. Gray matter regions included globus pallidus, putamen, thalamus (ventral anterior nucleus), caudate nucleus, dentate nucleus, amygdala, frontal-, temporal-, occipital- and cerebellar cortex. White matter samples were collected from frontal-, temporal- and occipital white matter, corpus callosum and cerebellar peduncle. All samples were coded for MRI and subsequent biochemical processing.

2.3. MRI data acquisition

2.3.1. *Postmortem* in situ *brain*

Postmortem MRI of the *in situ* aceruloplasminemia brain was performed within 36 h of death. The subject was scanned at room temperature on a 3 T GE Discovery MR750 scanner (Waukesha, Milwaukee, USA), using a GE 16-channel Head Neck Spine (HNS) coil. T_2^* relaxation data were acquired using an axial 3D multi-echo gradient echo sequence with 8 echoes (range 3–21.5 ms, repetition time 32.2 ms, flip angle 15°, spatial resolution 1 mm × 1 mm × 2 mm). This acquisition protocol was comparable to that used in the Erasmus MC for *in vivo* imaging of patients with aceruloplasminemia. An axial ultra-short echo time (3D UTE) gradient echo sequence with 2 echoes was additionally acquired (range 0.032 ms – 3 ms, repetition time 9 ms, flip angle 5°, spatial resolution 0.4 mm × 0.4 mm × 3 mm). This sequence had not yet been implemented in clinical practice, and its much higher in-plane resolution was primarily chosen to better visualize the distribution of iron in the most heavily iron-loaded brain regions.

2.3.2. *Brain slabs*

Before dissection of the samples, high resolution MRI of the aceruloplasminemia brain slabs was performed. The slabs were arranged side by side, covered in plastic and scanned at room temperature on a 3 T GE Discovery MR750 scanner (Waukesha, Milwaukee, USA), using a NeoCoil 16-channel GEM Flex small coil (Pewaukee, Wisconsin, USA). The imaging protocol consisted of a coronal 3D multi-echo gradient echo sequence with 3 echoes (range 6.1–25.7 ms, repetition time 32.4 ms, flip angle 40°, 0.2 mm × 0.2 mm × 0.1 mm spatial resolution).

2.3.3. *Tissue samples*

Dissected tissue blocks from both the aceruloplasminemia and control subject were put in 2 ml tubes and immersed in 4% phosphate buffered formaldehyde. The 100 tubes were placed in a plastic sample holder that was filled with Milli-Q water® (Millipore, USA) to further avoid susceptibility artefacts due to surrounding air. MRI was performed at room temperature on a 1.5 T GE Artist scanner using a NeoCoil 16-channel GEM Flex small coil (Pewaukee, Wisconsin, USA). 1.5 T was chosen instead of 3 T given the extremely fast signal decay that was observed in some deep gray matter regions of the aceruloplasminemia brain during *in situ* imaging. T_2^* relaxation data were acquired using one axial 3D multi-echo gradient echo sequence with 16 echoes (range 3.3–49.1 ms, repetition time 78 ms, flip angle 60°, spatial resolution 0.5 mm × 0.5 mm × 0.3 mm) and two 3D UTE sequences: a short TE variation with 11 echoes (range 0.032–5 ms, steps of 0.5 ms, repetition time 14 ms, flip angle 20°, 0.6 mm^3 isotropic spatial resolution) and a long TE variation with 7 echoes (range 0.032–18 ms, with TEs at 0, 1, 2, 4, 8, 12 and 18 ms, repetition time 26.4 ms, flip angle 20° and 0.6 mm^3 isotropic spatial resolution).

2.4. MRI data analysis

2.4.1. *Postmortem* in situ *brain*

The *in situ* R_2^* map of the aceruloplasminemia subject was calculated from the 3D multi-echo gradient echo data, using the three-parameter fitting algorithm within the AW Server software package (version 2.0, GE Healthcare, Waukesha, Milwaukee, USA): $y = A \bullet e^{-TE \bullet R2*} + B$, where A is the initial signal intensity, and B is the offset signal of the system. To facilitate comparisons between the *in situ* R_2^* data and R_2^* obtained from the tissue samples – *sample* R_2^*, the *in situ* R_2^* map was manually transformed with 3D Slicer (Slicer, version 4.11) (Fedorov et al., 2012) to match the coronal orientation and angulation of the brain slab of which the basal ganglia samples were taken. The high-resolution image of this brain slab was used as a reference. For each sample of which the approximate sampling location could be identified based on anatomical landmarks, a rectangular 2D region of interest (ROI) was manually drawn on the transformed *in situ* image that was most similar to the surface of the sectioned brain slab, using the ROI manager tool within ImageJ (Schneider et al., 2012). This ROI was propagated to three adjacent *in situ* images, on average, depending on the dimensions of the sample. These dimensions were accurately verified by using photographs of the sectioned brain slab. Mean intensity values of each ROI were extracted, and subsequently averaged to obtain mean *in situ* R_2^* for each sample. Standard deviations were obtained accordingly.

The data analysis of the postmortem *in situ* MRI of the aceruloplasminemia subject is summarized in Fig. 1.

2.4.2. *Tissue samples*

Mean *sample* R_2^* and its standard deviation were calculated for each entire tissue block of the aceruloplasminemia and control subject, by using the same three-parameter fitting algorithm as described above, where the offset term captures the echoes laying in the noise. Note that, for both subjects, the assumption of mono-exponentiality was verified in tissue samples of the most heavily iron-loaded brain regions. Some examples for the aceruloplasminemia subject are shown in the Supplementary Material (Figure S1).

2.5. Biochemical analysis

Following MRI, residual formalin was removed. Tissue specimens were washed with Milli-Q® water (Millipore, USA) and destructed according to the method previously described (Kumar et al., 2016). The volumes of the destructives were tripled compared to the described method to account for the higher amounts of tissue in our study (36–214 mg fixed wet weight). The specimens were destroyed using 900 µl nitric acid 65% (Suprapur®, Merck, Germany) at 90 °C for 2 h. To ensure total tissue destruction, 300 µl hydrogen peroxide 30% (Suprapur®, Merck, Germany) was added and the solution was heated again at 90 °C for 1 h. After cooling down, the tubes were filled with Milli-Q® water till 15 ml. Two blank solutions with reagents only, a solution with fresh formalin and a solution with formalin that was used for fixation of the aceruloplasminemia tissue were prepared accordingly.

National Institute of Standards and Technology (NIST)-traceable 1000 mg/L elemental standards were used (TraceCERT®, Fluka) for preparation of the iron calibration standards and internal standards. Calibration standards were prepared in a Secuflow fumehood (SCALA) to prevent contamination by atmospheric particulates. Five external iron calibration standards were prepared: 0, 50, 200, 1000, 5000 µg/L. 10 µg/L Rh and In were used as internal standards. The standards and tissue samples were analyzed for trace elements using the NexION® 2000 (PerkinElmer, USA) ICP-MS equipped with a concentric glass nebulizer and Peltier-cooled glass spray chamber. An SC2 DX autosampler (PerkinElmer, USA) was connected to the ICP-MS for sample introduction. Syngistix™ Software for ICP-MS (v.2.5, PerkinElmer, USA) was used for all data recording and processing. Trace iron concentrations were determined using the kinetic energy discrimination (KED) mode with 10% helium gas to minimize polyatomic interferences. The calibration was verified by including a blank measurement and a repeated measurement of one of the calibration standards, and required a correlation coefficient of ≥ 0.999. Matrix-related effects on the analyte signal were excluded by the analysis of a spiked destructed tissue sample.

All raw data are openly available upon request.

2.6. Statistics

Statistical analyses were performed using SPSS Version 25 (IBM, Armonk, NY). Tissue samples were categorized into different brain regions, for which median (interquartile range) iron concentrations and R_2^* values were reported. Linear regression analyses were used to determine the relationship between iron content and *sample* R_2^*, separately for gray and white matter, between *in situ* R_2^* and *sample* R_2^* for gray matter samples of the aceruloplasminemia brain, and between iron content and *in situ* R_2^* for gray matter samples of the aceruloplasminemia brain. An analysis of covariance was used to test for significant differences between the regression slopes for gray and white matter. Statistical significance was defined as $p \leq 0.05$.

3. Results

3.1. Biochemical analysis

Biochemical analysis of 100 brain tissue samples, including 34 gray matter and 16 white matter specimens of both the aceruloplasminemia and control subject, showed that for all brain regions the median brain iron concentration in aceruloplasminemia was at least ten times higher than in the control subject. In the deep gray matter, median iron concentrations in aceruloplasminemia reached above 15 times the normal concentration, with the dentate nucleus being by far the most heavily iron-loaded structure (Fig. 2).

Table 1 summarizes the iron concentrations separately for each brain region. Deep gray matter brain structures in aceruloplasminemia showed large intra-structural variations in iron content. The dentate nucleus reached a maximum iron content of 4184 mg/kg wet tissue, with a median iron concentration of over 2500 mg/kg, followed by a median iron concentration of over 700 mg/kg in the putamen. These values are substantially higher than in the control subject, where the highest iron concentration was found in the globus pallidus and reached 65 mg/kg, with a median iron concentration around 50 mg/kg. Cortical iron accumulation in aceruloplasminemia was most prominent in the cerebellar cortex, followed by the occipital cortex, temporal cortex, and frontal cortex. In white matter, the cerebellar peduncle was most heavily iron-loaded, followed by the temporal white matter, corpus callosum, frontal white matter and occipital white matter (Supplementary Material, Table S1).

Formalin that was used to store the aceruloplasminemia brain tissue showed a nearly nine-fold increase in iron concentration compared to fresh formalin (4.0 mg/l vs. 0.5 mg/l, respectively).

3.2. MRI data

For aceruloplasminemia tissue samples with an iron concentration up to 1000 mg/kg, R_2^* could be reliably calculated from the 3D multi-echo gradient echo sequence at 1.5 T (Table 1). The extremely iron-loaded dentate nucleus had a signal decay too fast to be adequately covered by this sequence, therefore we used a UTE sequence for this region. The UTE sequence with TE variation from 0 ms to 5 ms at 1.5 T best covered the echo decay for the dentate nucleus samples of the aceruloplasminemia subject (Supplementary Material, Figure S2). Visual inspection of the postmortem *in situ* dual-echo UTE data suggests that UTE sequences also have the potential to provide useful R_2^* results for these most heavily iron-loaded brain regions *in situ* (Fig. 3).

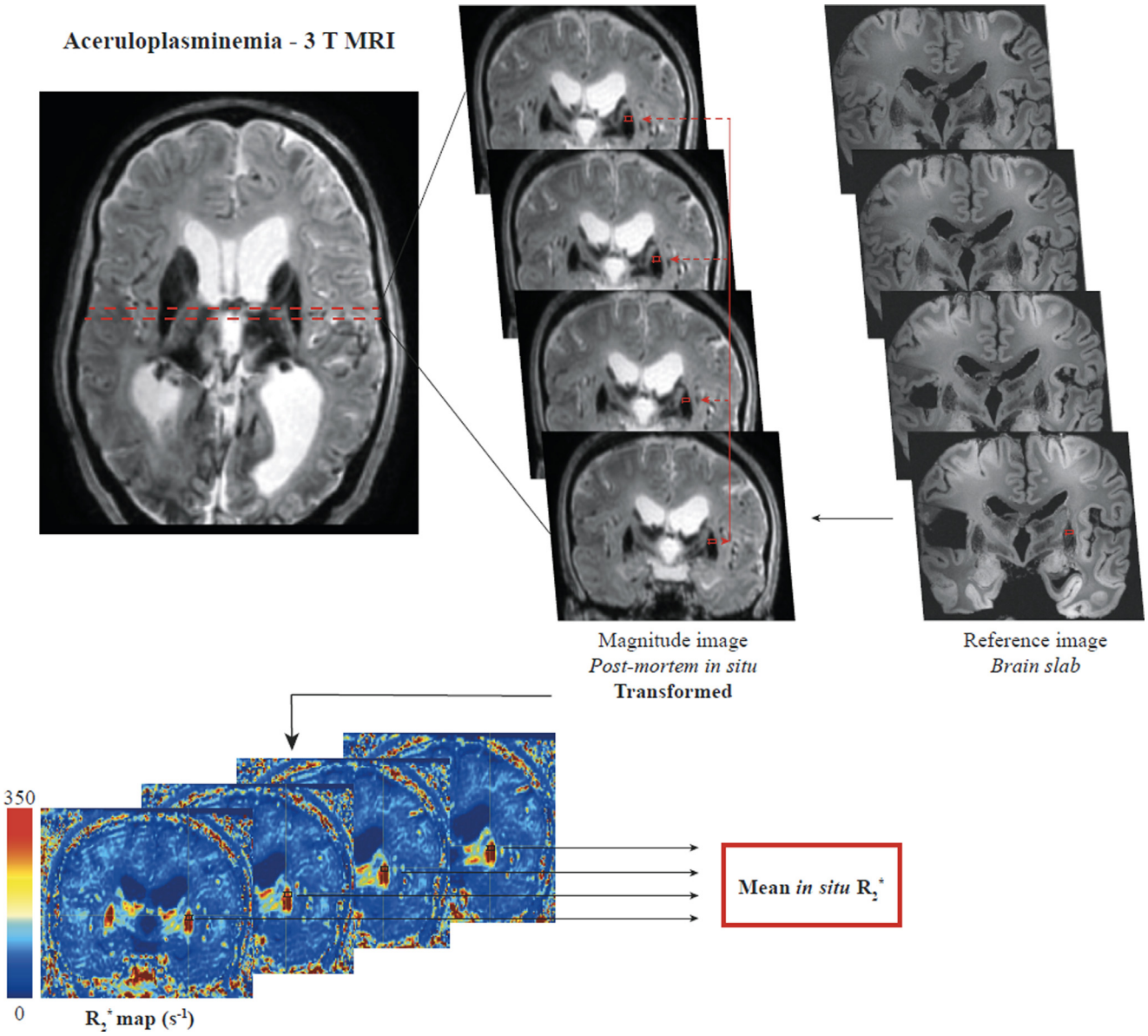

Fig. 1. MRI data analysis of the postmortem *in situ* aceruloplasminemia brain.
The high-resolution MR image of the brain slab containing the basal ganglia (TE = 6.1 ms) was used as a reference to appropriately align the coronal orientation and angulation of the postmortem *in situ* MRI (TE = 10.9) with that of the brain slab (3D Slicer). Rectangular regions of interest (ROIs), which were in correspondence with the dimensions of the samples, were manually drawn on the transformed magnitude images and subsequently projected on the R_2^* map (ImageJ). The results of these ROIs were averaged to obtain mean *in situ* R_2^* - here shown for one of the left putaminal samples.

Table 1
Iron concentrations by ICP-MS and R_2^* at 1.5 T in aceruloplasminemia and control brain samples.

Brain region	Number of samples*	Iron concentration (mg/kg wet weight)		$R_2^*(s^{-1})$	
		ACP	Control	ACP	Control
Dentate nucleus	4	2576 (1912–3645)	28 (26–36)	475 (379–745)†	48 (47–51)
Putamen	4	741 (687–822)	40 (38–46)	164 (149–170)	35 (33–37)
Thalamus	2	580 (481–679)	37 (31–43)	132 (111–152)	42 (41–43)
Caudate nucleus	2	506 (482–529)	45 (43–46)	90 (88–93)	39 (38–39)
Globus pallidus	4	485 (441–592)	49 (41–61)	111 (103–130)	42 (39–65)
Cortex	16	411 (378–443)	36 (32–39)	78 (73–88)	34 (32–36)
Amygdala	2	314 (308–319)	29 (28–29)	66 (64–67)	35 (30–39)
White matter	16	309 (215–394)	31 (24–34)	76 (70–99)	48 (46–53)

Abbreviations: ACP – aceruloplasminemia. Data are expressed as median (interquartile range) values.
* Number of samples for each subject. †R_2^* derived from the UTE sequence with TE variation 0 ms - 5 ms, as the signal decay was too fast to be covered by the 3D multi-echo gradient echo sequence at 1.5 T.

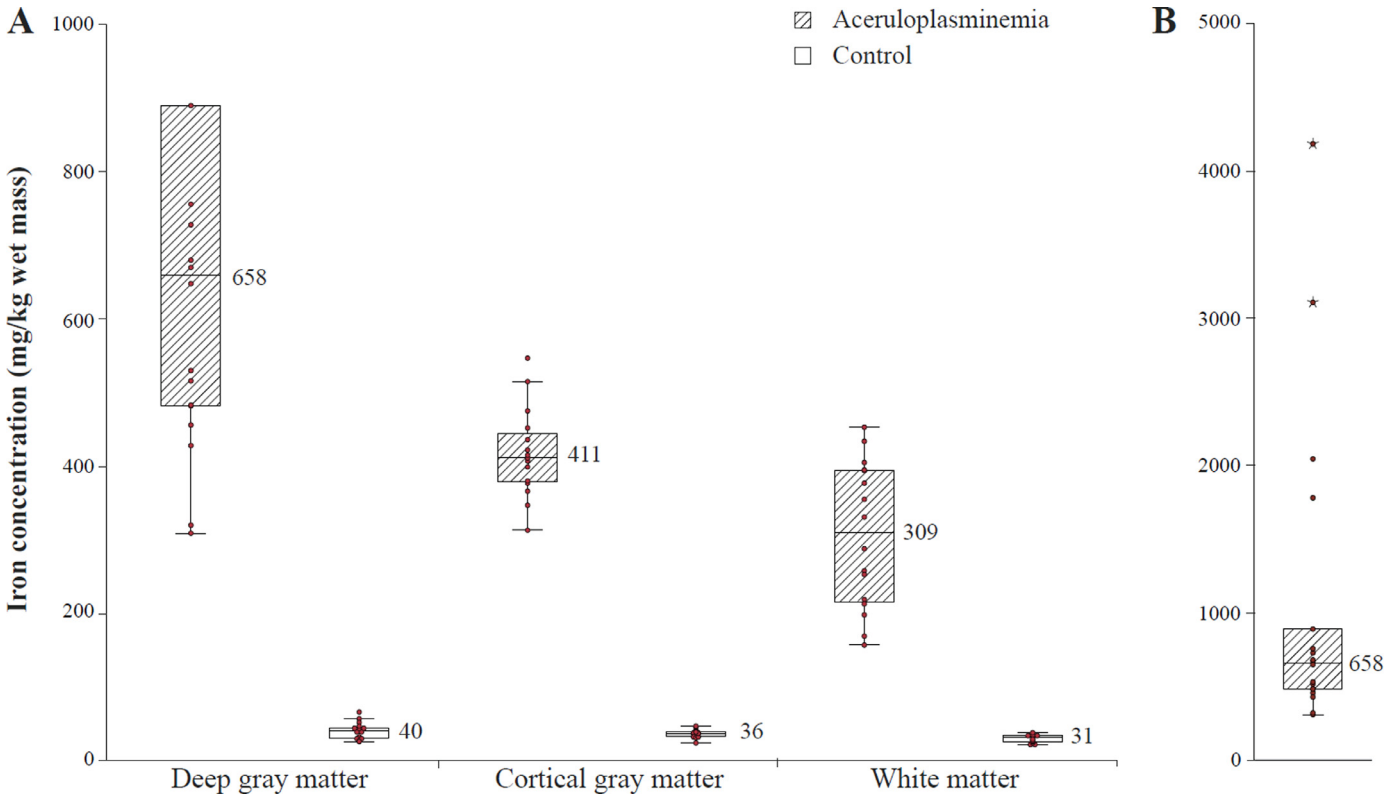

Fig. 2. Iron concentrations by ICP-MS for various brain regions of the aceruloplasminemia and control brain.
Deep gray matter regions include basal ganglia, dentate nucleus, amygdala and thalamus. The boxplots represent median iron concentrations, together with the interquartile ranges. The whiskers represent values within the 1.5-fold interquartile range (A). Panel B shows the dentate nucleus samples of the aceruloplasminemia brain as outliers above the 1.5-fold interquartile range (dots) and 5-fold interquartile range (stars) of deep gray matter regions.

The relationship between iron content and *sample* R_2^* at 1.5 T for aceruloplasminemia tissue samples is shown in Fig. 4. For gray matter structures of the aceruloplasminemia brain with an iron concentration up to 1000 mg/kg, 91% of variation in R_2^* could be explained by iron and R_2^* increased with 0.21 s^{-1} for every mg iron/kg brain tissue ($p < 0.001$). The dentate nucleus was excluded from the linear regression analyses because its R_2^* values were obtained using a separate UTE sequence, as described above, which was not applicable to the rest of the tissue samples. Still, its R_2^* values followed the same slope (Supplementary Material, Figure S3). R_2^* was slightly less sensitive to variations in iron concentration in white matter, with a slope of 0.16 s^{-1} • kg/mg ($p < 0.001$). The regression slope for white matter was significantly different from the regression slope for gray matter ($p = 0.041$). No significant association was found between R_2^* and tissue iron content of the control samples (data not shown) .

For the 15/30 gray matter samples of the aceruloplasminemia subject that could be clearly identified on the postmortem *in situ* images, *in situ* R_2^* at 3 T and *sample* R_2^* at 1.5 T were highly correlated, as illustrated in Fig. 5A.). For white matter, the relationship between *in situ* R_2^* at 3 T and *sample* R_2^* at 1.5 T was not formally assessed, given only four white matter samples could be clearly identified on the postmortem *in situ* images. The change in R_2^* from *in situ* at 3 T to sample-based analysis after fixation at 1.5 T was different for cortex and white matter compared to deep gray matter, though, as illustrated in Fig. 5B.

The relationship between iron content and *in situ* R_2^* at 3 T for the 15 gray matter samples is shown in Fig. 6, and yielded a slope of 0.63 s^{-1} • kg/mg ($p < 0.001$).

4. Discussion

Evaluating the relationship between R_2^* and biochemically determined iron concentrations in postmortem aceruloplasminemia brain tissue, we may conclude that R_2^* might be used as a non-invasive measure of brain iron content in aceruloplasminemia and potentially other disorders within this spectrum of severe brain iron accumulation.

Although the deep gray matter structures in aceruloplasminemia were most heavily iron-loaded, with median iron concentrations reaching above 15 times the normal concentration, our work highlights that iron accumulation in aceruloplasminemia occurs throughout the whole brain and also involves cortex and white matter (Miyajima et al., 2003; Morita et al., 1995; Miyajima, 2015). R_2^* was highly sensitive to variations in iron content, both for affected gray and white matter samples. The strong association between *sample* R_2^* and *in situ* R_2^* for gray matter regions of the aceruloplasminemia brain confirms that the contrast differences that were found in the sample-based analysis are representative of the *in situ* brain.

The presented calibration equations, though, should be cautiously used to predict absolute brain iron concentrations *in vivo*. When comparing the relationship between iron content and *sample* R_2^* at 1.5 T with the relationship between iron content and *in situ* R_2^* at 3 T, differences in the regression slopes are indicative of some confounders. In fact, given that R_2^* is linearly related to the magnetic field from 1.5 T to 3 T (Yao et al., 2009; Peters et al., 2007), the slope of 0.21 s^{-1} • kg/mg that was determined for gray matter samples at 1.5 T should equate to a slope of 0.42 s^{-1} • kg/mg at 3 T. Our much steeper slope of 0.63 s^{-1} • kg/mg at 3 T is probably due to leakage of iron from the tissue during the five-year interval between postmortem *in situ* imaging and biochemical analysis of the tissue (Schrag et al., 2010; Gellein et al., 2008). Although this does not apply to the sample-based analysis, the converging behavior of R_2^* from 3 T to 1.5 T that was observed for deep gray matter structures compared to the cortex and white matter suggests fixation-related changes of the latter. While some convergence of the transverse relaxation times for deep gray matter compared to cortex and white matter has also been observed after fixation in controls (Birkl et al., 2016; Blamire et al., 1999), it is well possible that NBIA

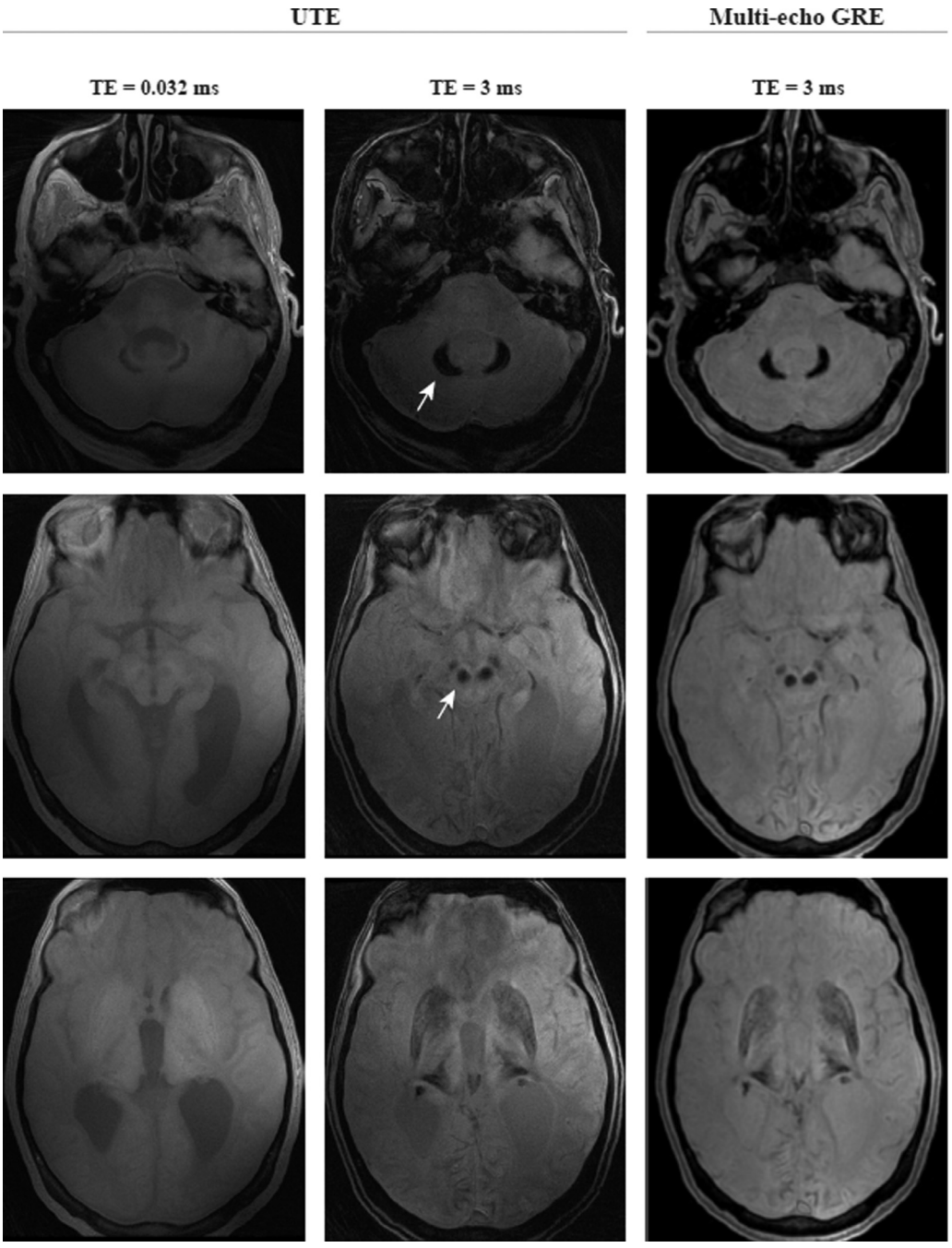

Fig. 3. Postmortem *in situ* UTE data at 3T for deep gray matter brain structures in aceruloplasminemia. A comparison between the TE = 0.032 ms and TE = 3 ms UTE data suggests that for the dentate nucleus (first row, white arrow), and for the red nucleus (second row, white arrow) – not biochemically analyzed in this study, $T_2^* < 3$ ms. Magnitude images obtained from the multi-echo gradient echo (GRE) sequence at TE = 3 ms for both regions and for the basal ganglia (third row) are provided for comparison.

areas with excess iron such as the deep gray matter would leak relatively more iron. Autolytic postmortem processes together with a lower tissue temperature might have additionally influenced our imaging results compared to *in vivo* (Birkl et al., 2016). It should be noted, though, that these limitations should be primarily considered when interpreting the shape of the relationship between tissue iron content and R_2^*. The sensitivity of R_2^* for variations in iron content, *i.e.* the strength of this relationship, is rather substantiated by the consistency that was observed between *in situ* R_2^* and *sample* R_2^*, predominantly among deep gray matter structures.

As such, R_2^* could be used to evaluate the iron content of deep gray matter brain structures in aceruloplasminemia, and as an outcome measure of iron chelation therapy. For that purpose, the selection of a region of interest that is representative of the structure should be a major concern, given the large intra-structural variation in iron content that was observed in our study. This underlines the importance of selecting a region of interest that covers the whole structure (Zhou et al., 2020), and of minimizing factors that might complicate reproducibility, such as differences in acquisition parameters or magnetic field strength between follow-up scans (Gracien et al., 2020).

The extremely fast signal decay is another challenge of using R_2^* as a measure of the iron content for deep gray matter brain structures in aceruloplasminemia on clinical scanners. Although this can be partially mitigated by the use of 1.5 T instead of 3 T MRI (Zhou et al.,

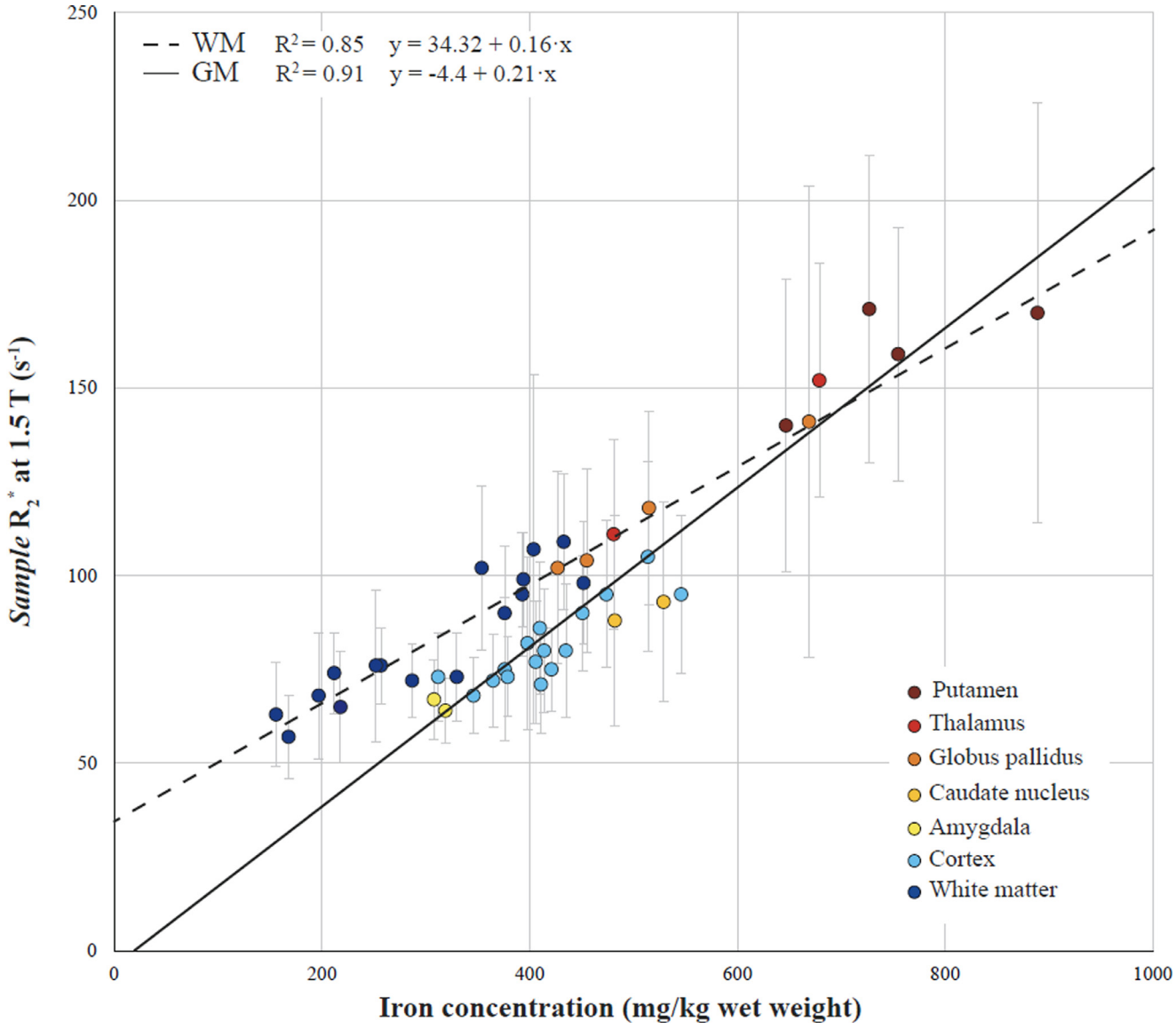

Fig. 4. Relationship between iron concentration and R_2^* at 1.5 T in aceruloplasminemia tissue samples.
The solid line represents the regression line for gray matter (GM). The dotted line represents the regression line for white matter (WM). The error bars represent the standard deviation of R_2^*.

2020; Labranche et al., 2018), even at 1.5 T our 3D multi-echo gradient echo sequence failed to capture the extreme iron-loading of the dentate nucleus in the studied aceruloplasminemia brain. Ultra-short echo time (UTE) sequences might enable evaluation of R_2^* for such extremely iron-loaded regions, as supported by both our quantitative analysis of the dentate nucleus samples at 1.5 T and qualitative observations *in situ* at 3 T. However, to our knowledge, the iron concentration of approximately 4000 mg/kg that was detected in one of the dentate nucleus samples of our aceruloplasminemia subject is the highest amount of iron that has ever been found in the human brain. Other NBIA studies estimated deep gray matter iron concentrations between 800 mg/kg and 1000 mg/kg (Dusek et al., 2014; Löbel et al., 2014), up to a four-fold lower. In all likelihood, routine gradient echo protocols with a relatively short echo time (~3 ms) at 1.5 T should suffice for most patients in clinical practice, and UTE protocols would only be required for extreme cases.

In fact, compared to previously reported R_2^* values for deep gray matter structures in patients with aceruloplasminemia *in vivo*, our postmortem *in situ* R_2^* values were approximately two times higher (Zhou et al., 2020; Pan et al., 2011). This might be explained by the longer duration of neurological manifestations in our subject compared to these previously reported patients, as both the severity of iron accumulation and its regional distribution have shown to expand with a longer duration of neurological manifestations (Kaneko et al., 2012). Although the loss of signal on T_2^*-weighted images that was observed within the dentate nucleus and red nucleus in one of the previously reported patients might suggest that these structures are preferentially affected in aceruloplasminemia (Zhou et al., 2020), it remains to be elucidated whether these findings indeed represent a common feature of the disease. Still, the regional distribution of iron seems different in aceruloplasminemia compared to the healthy situation, with the lateral division of the thalamus being remarkably iron-loaded (Vroegindeweij et al., 2017; Vroegindeweij et al., 2021; Miyajima, 2015; Kim et al., 2017), while the globus pallidus may be relatively iron-spared (Zhou et al., 2020; Salsone et al., 2021).

Apart from the fixation-related caveats of our work that have been described above, several other limitations should be considered. Firstly, the slope of the relationship between tissue iron content and R_2^* in the studied aceruloplasminemia brain could not be directly compared

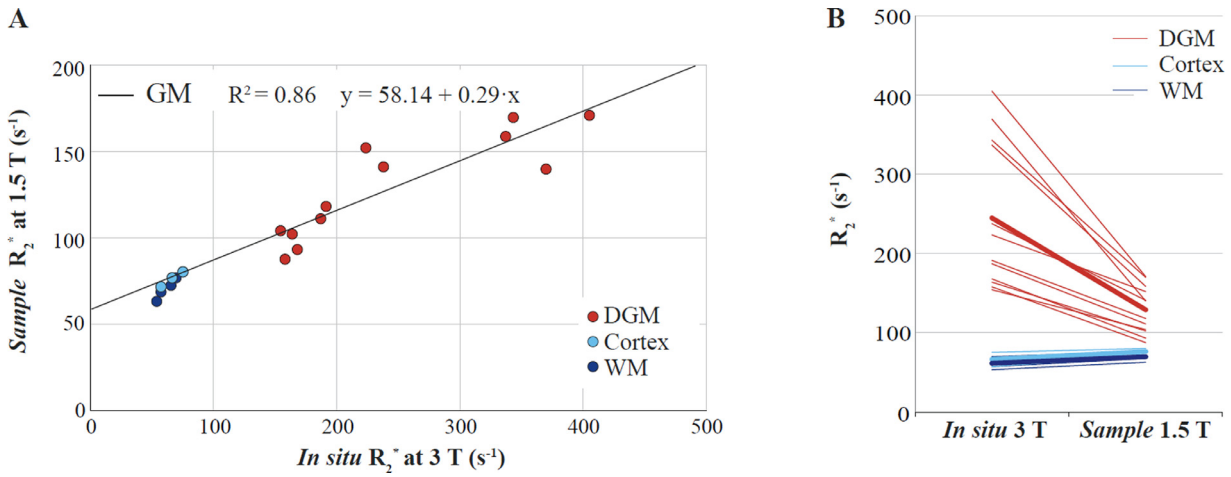

Fig. 5. Comparison between "*in situ*" R_2^* and "sample" R_2^* for gray and white matter brain regions in aceruloplasminemia.
"In situ" R_2^* was highly correlated with "sample" R_2^* for 15 gray matter regions that could be clearly identified on the postmortem *in situ* MRI. The relationship between "*in situ*" R_2^* at 3 T and "sample" R_2^* at 1.5 T was not formally assessed for white matter, given only four white matter data points could be included (A). Panel B indicates the change in R_2^* from *in situ* imaging at 3T to sample imaging at 1.5 T for deep gray matter (red lines), cortex (light blue lines) and white matter samples (dark blue lines). The bold lines represent the average change in R_2^* for deep gray matter samples (DGM) – ratio 0.53, cortex samples – ratio 1.15, and white matter samples (WM) – ratio 1.13 .

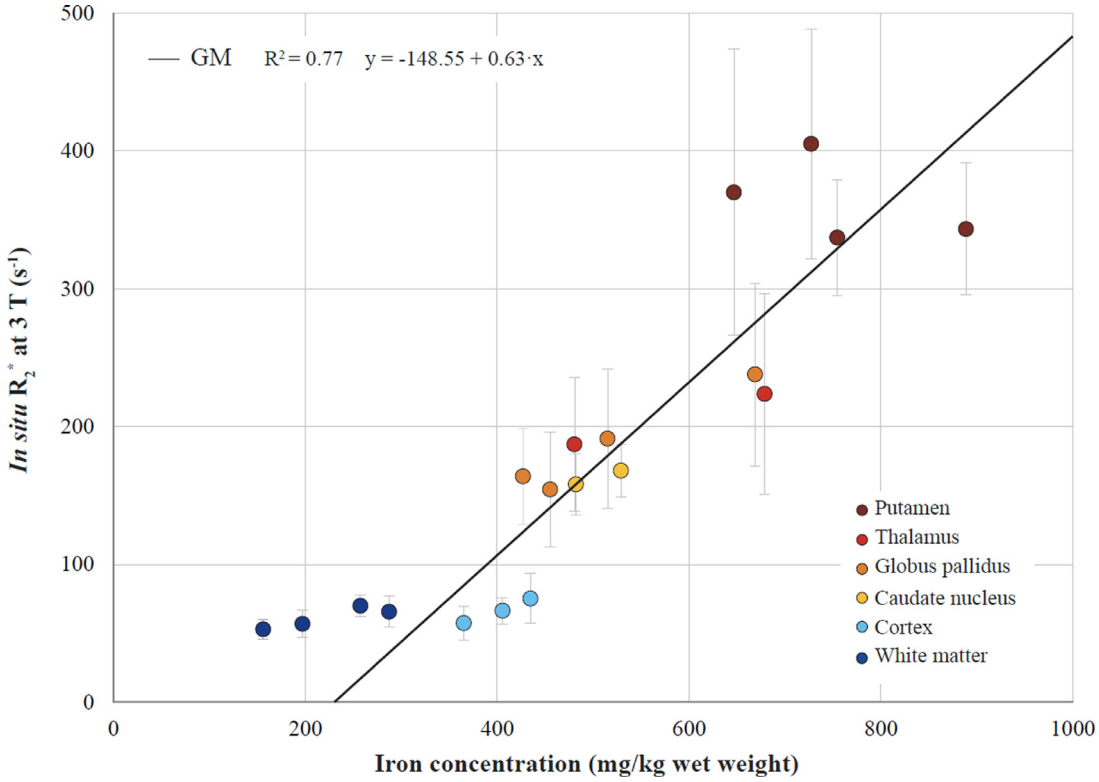

Fig. 6. Relationship between iron concentration and "*in situ*" R_2^* at 3 T for aceruloplasminemia gray matter samples. The error bars represent the standard deviation of R_2^*. Linear regression analysis was not performed separately for white matter, given only four white matter data points could be included.

to that in control subjects. While methodological differences and much shorter durations of formalin fixation hindered appropriate comparisons with previously reported iron-R_2^* calibrations in control subjects (Langkammer et al., 2010; Stuber et al., 2014; Hametner et al., 2018), no significant association was found between control iron content and *sample* R_2^* in this work. The latter might be due to the relatively small range and low iron concentrations that were measured in the control brain samples (Langkammer et al., 2010; Hametner et al., 2018). Potential differences in the regression slope between patients with aceruloplasminemia and healthy subjects might be due to clustering of iron particles (Gossuin et al., 2007), and/or the coexistence of different molecular iron forms with varying magnetic properties (Dezortova et al., 2012; Birkl et al., 2020; Dietrich et al., 2017). Significant influences of changes in the oxidation state of iron, though, were not substantiated by our previous study that directly quantified specific molecular iron forms in the same subject with aceruloplasminemia (Vroegindeweij et al., 2021), nor by non-monoexponentiality of the transverse magnetization decay in this work. Still, additional T_2 sequences would have been of interest,

since analyses of the spin-echo decay could reveal relevant information on the clustering of iron particles (Jensen et al., 2010), and the combination of R_2 and R_2^* maps could provide valuable insights into the size of these particles (Lee et al., 2018). Moreover, R_2 might be considered as a measure of brain iron content for those extremely iron-loaded regions that could not generate useful R_2^* results using conventional gradient echo sequences at 1.5 T.

The lack of quantitative susceptibility mapping (QSM) is another limitation of our study, as QSM also has the potential to quantify the iron content in extremely iron-loaded regions where the signal decay is too fast to generate useful R_2^* results (Haacke et al., 2015). On the other hand, the at least ten-fold increase in iron content throughout the whole aceruloplasminemia brain, and the resulting lack of a zero reference region, may easily bias the relative differences in magnetic susceptibility among brain regions that are normally exploited by QSM (Zhou et al., 2020; Langkammer et al., 2012).

In conclusion, R_2^* is now validated as a measure of brain iron content for heavily iron-loaded deep gray matter brain structures in aceruloplasminemia, and potentially also other forms of NBIA. We show that R_2^* linearly correlates with iron concentration, and may therefore provide a useful quantifiable biomarker to evaluate disease progression and outcomes of iron chelation therapy *in vivo*. Routine gradient echo protocols with a first echo time ~3 ms at 1.5 T are recommended.

Data availability

All raw data are openly available upon request.

Declaration of Competing Interest

None.

Credit authorship contribution statement

Lena H.P. Vroegindeweij: Conceptualization, Methodology, Resources, Formal analysis, Writing – original draft, Visualization, Project administration. **Piotr A. Wielopolski:** Methodology, Investigation, Writing – review & editing. **Agnita J.W. Boon:** Conceptualization, Writing – review & editing. **J.H. Paul Wilson:** Conceptualization, Writing – review & editing. **Rob M. Verdijk:** Resources, Investigation, Writing – review & editing. **Sipeng Zheng:** Methodology, Investigation, Writing – review & editing. **Sylvestre Bonnet:** Methodology, Investigation, Writing – review & editing. **Lucia Bossoni:** Methodology, Writing – review & editing. **Louise van der Weerd:** Methodology, Writing – review & editing. **Juan A. Hernandez-Tamames:** Methodology, Investigation, Writing – review & editing. **Janneke G. Langendonk:** Conceptualization, Methodology, Writing – review & editing, Supervision.

Acknowledgments

The authors are very grateful to the patient with aceruloplasminemia and his family to agree with this research, would like to thank M. Bulk, C. Langkammer and W. Goessler for useful discussions and for sharing their protocol on tissue preparation for ICP-MS, L. van der Zee and K. Dorst for assistance with the preparation, coding and storage of the tissue samples for ICP-MS, D. Papp for assistance with MR image analyses, and H. Qi for advice on statistical analyses.

Ethical approval

The study of the patient with aceruloplasminemia was approved by the Medical Ethics Review Board of the Erasmus MC (approval number: MEC-2011-525). The control subject provided written informed consent for the secondary use of the tissue for research purposes, and all tissue was handled in a coded fashion according to the Dutch National Ethical Guidelines (Code for Proper Secondary Use of Human Tissue, Dutch Federation of Medical Scientific Societies).

Funding

This study was partly supported by the Netherlands Organization for Scientific Research (NWO) through a VENI fellowship to L.B. (0.16.Veni.188.040).

Supplementary materials

Supplementary material associated with this article can be found, in the online version, at doi:10.1016/j.neuroimage.2021.118752.

References

Miyajima, H., Takahashi, Y., Aceruloplasminemia, K.S., 2003. an inherited disorder of iron metabolism. Biometals 16 (1), 205–213.
Morita, H., Ikeda, S., Yamamoto, K., Morita, S., Yoshida, K., Nomoto, S., et al., 1995. Hereditary ceruloplasmin deficiency with hemosiderosis: a clinicopathological study of a Japanese family. Ann. Neurol. 37 (5), 646–656.
Langkammer, C., Krebs, N., Goessler, W., Scheurer, E., Ebner, F., Yen, K., et al., 2010. Quantitative MR imaging of brain iron: a postmortem validation study. Radiology 257 (2), 455–462.
Stuber, C., Morawski, M., Schafer, A., Labadie, C., Wahnert, M., Leuze, C., et al., 2014. Myelin and iron concentration in the human brain: a quantitative study of MRI contrast. Neuroimage 93 (Pt 1), 95–106.
Hametner, S., Endmayr, V., Deistung, A., Palmrich, P., Prihoda, M., Haimburger, E., et al., 2018. The influence of brain iron and myelin on magnetic susceptibility and effective transverse relaxation - A biochemical and histological validation study. Neuroimage 179, 117–133.
Bulk, M., Abdelmoula, W.M., Geut, H., Wiarda, W., Ronen, I., Dijkstra, J., et al., 2020. Quantitative MRI and laser ablation-inductively coupled plasma-mass spectrometry imaging of iron in the frontal cortex of healthy controls and Alzheimer's disease patients. Neuroimage 215, 116808.
Dusek, P., Tovar Martinez, E.M., Madai, V.I., Jech, R., Sobesky, J., Paul, F., et al., 2014. 7-tesla magnetic resonance imaging for brain iron quantification in homozygous and heterozygous PANK2 mutation carriers. Mov. Disord. Clin. Pract. 1 (4), 329–335.
Löbel, U., Schweser, F., Nickel, M., Deistung, A., Grosse, R., Hagel, C., et al., 2014. Brain iron quantification by MRI in mitochondrial membrane protein-associated neurodegeneration under iron-chelating therapy. Ann. Clin. Transl. Neurol. 1 (12), 1041–1046.
Chavhan, G.B., Babyn, P.S., Thomas, B., Shroff, M.M., Haacke, E.M., 2009. Principles, techniques, and applications of T2*-based MR imaging and its special applications. Radiographics 29 (5), 1433–1449.
Li, T.Q., Yao, B., van Gelderen, P., Merkle, H., Dodd, S., Talagala, L., et al., 2009. Characterization of T(2)* heterogeneity in human brain white matter. Magn. Reson. Med. 62 (6), 1652–1657.
Gossuin, Y., Gillis, P., Muller, R.N., Hocq, A., 2007. Relaxation by clustered ferritin: a model for ferritin-induced relaxation *in vivo*. NMR Biomed. 20 (8), 749–756.
Tanimoto, A., Oshio, K., Suematsu, M., Pouliquen, D., Stark, D.D., 2001. Relaxation effects of clustered particles. J. Magn. Reson. Imaging 14 (1), 72–77.
Klopstock, T., Tricta, F., Neumayr, L., Karin, I., Zorzi, G., Fradette, C., et al., 2019. Safety and efficacy of deferiprone for pantothenate kinase-associated neurodegeneration: a randomised, double-blind, controlled trial and an open-label extension study. Lancet Neurol. 18 (7), 631–642.
Zhou, L., Chen, Y., Li, Y., Gharabaghi, S., Chen, Y., Sethi, S.K., et al., 2020. Intracranial iron distribution and quantification in aceruloplasminemia: a case study. Magn. Reson. Imaging 70, 29–35.
Pan, P.L., Tang, H.H., Chen, Q., Song, W., Shang, H.F., 2011. Desferrioxamine treatment of aceruloplasminemia: long-term follow-up. Mov. Disord. 26 (11), 2142–2144.
Zorzi, G., Zibordi, F., Chiapparini, L., Bertini, E., Russo, L., Piga, A., et al., 2011. Iron-related MRI images in patients with pantothenate kinase-associated neurodegeneration (PKAN) treated with deferiprone: results of a phase II pilot trial. Mov. Disord. 26 (9), 1756–1759.
Cossu, G., Abbruzzese, G., Matta, G., Murgia, D., Melis, M., Ricchi, V., et al., 2014. Efficacy and safety of deferiprone for the treatment of pantothenate kinase-associated neurodegeneration (PKAN) and neurodegeneration with brain iron accumulation (NBIA): results from a four years follow-up. Parkinsonism Relat. Disord. 20 (6), 651–654.
Abbruzzese, G., Cossu, G., Balocco, M., Marchese, R., Murgia, D., Melis, M., et al., 2011. A pilot trial of deferiprone for neurodegeneration with brain iron accumulation. Haematologica 96 (11), 1708–1711.
Vroegindeweij, L.H., van der Beek, E.H., Boon, A.J., Hoogendoorn, M., Kievit, J.A., Wilson, J.H., et al., 2015. Aceruloplasminemia presents as Type 1 diabetes in non-obese adults: a detailed case series. Diabet. Med. 32 (8), 993–1000.
Vroegindeweij, L.H.P., Langendonk, J.G., Langeveld, M., Hoogendoorn, M., Kievit, A.J.A., Di Raimondo, D., et al., 2017. New insights in the neurological phenotype of aceruloplasminemia in Caucasian patients. Parkinsonism Relat. Disord. 36, 33–40.
Kerkhof, M., Honkoop, P., 2014. Never forget aceruloplasminemia in case of highly suggestive Wilson's disease score. Hepatology 59 (4), 1645–1647.
Vroegindeweij, L.H.P., Boon, A.J.W., Wilson, J.H.P., Langendonk, J.G., 2020. Effects of iron chelation therapy on the clinical course of aceruloplasminemia: an analysis of aggregated case reports. Orphanet. J. Rare Dis. 15 (1), 105.
Vroegindeweij, L.H.P., Bossoni, L., Boon, A.J.W., Wilson, J.H.P., Bulk, M., Labra–Muñoz, J., et al., 2021. Quantification of different iron forms in the aceruloplasminemia brain to explore iron-related neurodegeneration. NeuroImage Clin. 30, 102657.

Fedorov, A., Beichel, R., Kalpathy-Cramer, J., Finet, J., Fillion-Robin, J.C., Pujol, S., et al., 2012. 3D Slicer as an image computing platform for the Quantitative Imaging Network. Magn. Reson. Imaging 30 (9), 1323–1341.
Schneider, C.A., Rasband, W.S., Eliceiri, K.W., 2012. NIH Image to ImageJ: 25 years of image analysis. Nat. Methods 9 (7), 671–675.
Kumar, P., Bulk, M., Webb, A., van der Weerd, L., Oosterkamp, T.H., Huber, M., et al., 2016. A novel approach to quantify different iron forms in ex-vivo human brain tissue. Sci. Rep. 6, 38916.
Miyajima, H, 2015. Aceruloplasminemia. Neuropathology 35 (1), 83–90.
Yao, B., Li, T.Q., Gelderen, P., Shmueli, K., de Zwart, J.A., Duyn, J.H., 2009. Susceptibility contrast in high field MRI of human brain as a function of tissue iron content. Neuroimage 44 (4), 1259–1266.
Peters, A.M., Brookes, M.J., Hoogenraad, F.G., Gowland, P.A., Francis, S.T., Morris, P.G., et al., 2007. T2* measurements in human brain at 1.5, 3 and 7 T. Magn. Reson. Imaging 25 (6), 748–753.
Schrag, M., Dickson, A., Jiffry, A., Kirsch, D., Vinters, H.V., Kirsch, W., 2010. The effect of formalin fixation on the levels of brain transition metals in archived samples. Biometals 23 (6), 1123–1127.
Gellein, K., Flaten, T.P., Erikson, K.M., Aschner, M., Syversen, T., 2008. Leaching of trace elements from biological tissue by formalin fixation. Biol. Trace Elem. Res. 121 (3), 221–225.
Birkl, C., Langkammer, C., Golob-Schwarzl, N., Leoni, M., Haybaeck, J., Goessler, W., et al., 2016. Effects of formalin fixation and temperature on MR relaxation times in the human brain. NMR Biomed. 29 (4), 458–465.
Blamire, A.M., Rowe, J.G., Styles, P., McDonald, B., 1999. Optimising imaging parameters for post mortem MR imaging of the human brain. Acta Radiol. 40 (6), 593–597.
Gracien, R.-.M., Maiworm, M., Brüche, N., Shrestha, M., Nöth, U., Hattingen, E., et al., 2020. How stable is quantitative MRI? – Assessment of intra- and inter-scanner-model reproducibility using identical acquisition sequences and data analysis programs. Neuroimage 207, 116364.
Labranche, R., Gilbert, G., Cerny, M., Vu, K.N., Soulières, D., Olivié, D., et al., 2018. Liver iron quantification with MR imaging: a primer for radiologists. Radiographics 38 (2), 392–412.
Kaneko, K., Hineno, A., Yoshida, K., Ohara, S., Morita, H., Ikeda, S., 2012. Extensive brain pathology in a patient with aceruloplasminemia with a prolonged duration of illness. Hum. Pathol. 43 (3), 451–456.
Kim, H.K., Ki, C.S., Kim, Y.J., Lee, M.S., 2017. Radiological findings of two sisters with aceruloplasminemia presenting with chorea. Clin. Neuroradiol. 27 (3), 385–388.
Salsone, M., Arabia, G., Annesi, G., Gagliardi, M., Nistico, R., Novellino, F., et al., 2021. Aceruloplasminemia: a multimodal imaging study in an Italian family with a novel mutation. Neurol. Sci..
Dezortova, M., Herynek, V., Krssak, M., Kronerwetter, C., Trattnig, S., Hajek, M., 2012. Two forms of iron as an intrinsic contrast agent in the basal ganglia of PKAN patients. Contrast Media Mol. Imaging 7 (6), 509–515.
Birkl, C., Birkl-Toeglhofer, A.M., Kames, C., Goessler, W., Haybaeck, J., Fazekas, F., et al., 2020. The influence of iron oxidation state on quantitative MRI parameters in post mortem human brain. Neuroimage 220, 117080.
Dietrich, O., Levin, J., Ahmadi, S.A., Plate, A., Reiser, M.F., Bötzel, K., et al., 2017. MR imaging differentiation of Fe(2+) and Fe(3+) based on relaxation and magnetic susceptibility properties. Neuroradiology 59 (4), 403–409.
Jensen, J.H., Tang, H., Tosti, C.L., Swaminathan, S.V., Nunez, A., Hultman, K., et al., 2010. Separate MRI quantification of dispersed (ferritin-like) and aggregated (hemosiderin–like) storage iron. Magn. Reson. Med. 63 (5), 1201–1209.
Lee, H., Baek, S.-.Y., SY, Chun, Lee, J.-.H., Cho, H., 2018. Specific visualization of neuromelanin-iron complex and ferric iron in the human post-mortem substantia nigra using MR relaxometry at 7T. Neuroimage 172, 874–885.
Haacke, E.M., Liu, S., Buch, S., Zheng, W., Wu, D., Ye, Y., 2015. Quantitative susceptibility mapping: current status and future directions. Magn. Reson. Imaging 33 (1), 1–25.
Langkammer, C., Schweser, F., Krebs, N., Deistung, A., Goessler, W., Scheurer, E., et al., 2012. Quantitative susceptibility mapping (QSM) as a means to measure brain iron? A post mortem validation study. Neuroimage 62 (3), 1593–1599.